# Synaptotagmin-$Ca^{2+}$ triggers two sequential steps in regulated exocytosis in rat PC12 cells: fusion pore opening and fusion pore dilation

Chih-Tien Wang, Jihong Bai, Payne Y. Chang, Edwin R. Chapman and Meyer B. Jackson

*Department of Physiology, University of Wisconsin Medical School, Madison, WI, USA*

**Synaptotagmin I (Syt I), the putative $Ca^{2+}$ sensor in regulated exocytosis, has two $Ca^{2+}$-binding modules, the C2A and C2B domains, and a number of putative effectors to which Syt I binds in a $Ca^{2+}$-dependent fashion. The role of $Ca^{2+}$ binding to these domains remains unclear, as efforts to address questions about $Ca^{2+}$-triggered effector interactions have led to conflicting results. We have studied the effects of $Ca^{2+}$ on fusion pores using amperometry to follow the exocytosis of single vesicles in real time and analyse the kinetics of fusion pore transitions. Elevating [$Ca^{2+}$] in permeabilized cells reduced the fusion pore lifetime, indicating an action of $Ca^{2+}$ during the actual fusion process. Analysing the $Ca^{2+}$ dependence of the fusion pore lifetime, together with the frequency of pore openings and the proportion of openings that close without dilating (kiss-and-run events) enabled us to resolve exocytosis into a sequence of kinetic steps representing functional transitions in the fusion pore. Fusion pore opening and dilation were both accelerated by $Ca^{2+}$, indicating separate $Ca^{2+}$ control over each of these steps. $Ca^{2+}$ ligand mutations in either the C2A or C2B domains of Syt I reduced fusion pore opening, but had opposite actions on the rate of fusion pore closure. These studies resolve two separate and distinct $Ca^{2+}$-triggered steps during regulated exocytosis. The C2A and C2B domains of Syt I have different actions during these steps, and these actions may be linked to their distinctive effector interactions.**

(Received 24 August 2005; accepted after revision 9 November 2005; first published online 17 November 2005)
**Corresponding author** M. Jackson: Department of Physiology, SMI 127, University of Wisconsin, 1300 University Ave., Madison, WI 53706, USA. Email: mjackson@physiology.wisc.edu

Although evidence that synaptotagmin I (Syt I) is a $Ca^{2+}$ sensor in exocytosis continues to mount, the mechanism of the transduction process remains poorly understood. Syt I employs two $Ca^{2+}$-binding modules, the C2A and C2B domains, to sense $Ca^{2+}$ and trigger membrane fusion (Perin *et al.* 1990; Jahn & Südhof, 1999; Koh & Bellen, 2003; Tucker *et al.* 2004). $Ca^{2+}$ binding to sites in these two domains triggers a number of interactions with putative molecular targets, including liposomes containing phosphatidyl serine (PS) (Brose *et al.* 1992; Chapman, 2002), liposomes containing phosphatidyl inositol bisphosphate ($PIP_2$), other molecules of Syt I, the SNARE proteins SNAP-25 and syntaxin, and complexes containing these proteins (Chapman, 2002). Studies in a variety of cell types have indicated that the binding of Syt I to these diverse targets contributes to the triggering of exocytosis (Fukuda *et al.* 1995; Fernandez-Chacon *et al.* 2001; Bai *et al.* 2004*b*), raising the question of how these multiple effector interactions are coordinated. In light of these findings exocytosis would appear to depend on a complex sequence of steps that arises through the orchestrated activity of a number of molecular components.

Amperometry is a technique that is well suited to unravelling such complex processes involving a temporal sequence of events. This electrochemical technique detects readily oxidized substances (e.g. noradrenaline) contained within vesicles, and resolves some of the critical steps of exocytosis. At the onset of exocytosis of a single vesicle, amperometry reveals the opening of a fusion pore as a prespike foot (PSF), which arises from the slow leakage of the vesicle content through an open fusion pore. Fusion pores can then either close to retain most of the vesicle content and produce a kiss-and-run event, or dilate to expel the entire vesicle content and produce a spike. Our analysis of the temporal sequence of fusion pore openings and spikes revealed two distinct $Ca^{2+}$-triggered steps in exocytosis. Thus, Syt I and $Ca^{2+}$ trigger both the opening of

 DOI: 10.1113/jphysiol.2005.097378

fusion pores and their subsequent dilation. Furthermore, the C2A and C2B domains of Syt I play different roles in these two steps.

## Methods

### Molecular biology

DNA constructs encoding wild-type Syt I (G374) and the mutants Syt I-D230S and Syt I-D363N (Wang *et al.* 2003*a*) were subcloned into pIRES2EGFP (Clontech) as described (Wang *et al.* 2001). The pIRES2EGFP vector allows transfected cells to be selected on the basis of fluorescence. Cells were transfected with 50 $\mu$g of DNA by electroporation using an ECM 830 electroporator (BTX Inc., San Diego, CA, USA) with 230 V, 5 ms pulses. Analysis of immunoblots calibrated against recombinant standards indicated that Syt I levels are ~7.5-fold higher in cells transfected with either wild-type or mutant Syt I, compared to control cells transfected with blank vector (Bai *et al.* 2004*b*).

### Cell culture

PC12 cells were plated at densities of 1.2–2 $\times 10^5$ per 35 mm dish and cultured in Dulbecco's modified Eagle's medium supplemented with 4.5 mg ml$^{-1}$ glucose, 3.7 mg ml$^{-1}$ $NaHCO_3$, 5% horse serum, and 5% iron-supplemented calf serum at 37°C in a 10% $CO_2$ atmosphere (Hay & Martin, 1992). Cells were loaded the day before experiments by incubation overnight with 1.5 mM noradrenaline and 0.5 mM ascorbate. Cells plated on coated dishes (50 $\mu$g ml$^{-1}$ poly D-lysine and collagen I) were permeabilized with a freeze–thaw cycle using liquid nitrogen (Klenchin *et al.* 1998; Wang *et al.* 2003*a*). Secretion was evoked in both intact and permeabilized cells using solutions applied from a micropipette positioned near a cell. Solutions were ejected with pressure (10–20 p.s.i.) gated by a Picospritzer (General Valve Corp, Fairfield, CT, USA). In intact cells, exocytosis was triggered by application of a high KCl solution (mM: 105 KCl, 5 NaCl, 1 $NaH_2PO_4$, 0.7 $MgCl_2$, 2 $CaCl_2$, 10 Hepes, pH 7.4). In permeabilized cells, exocytosis was triggered by application of a solution consisting of (mM): 121 K-glutamate, 20 K-acetate, 0.2 EGTA, 20 Hepes, pH 7.2, with $Ca^{2+}$ adjusted to the desired concentration and verified with a $Ca^{2+}$ electrode.

### Amperometry and data analysis

Noradrenaline release was monitored by amperometry (Chow & von Rüden, 1995; Wang *et al.* 2001). Currents were recorded using 5 $\mu$m carbon fibre electrodes polarized at 650 mV with a VA-10 amplifier (ALA Scientific Instruments, Westbury, NY, USA). Signals were low-passed filtered at 1 kHz and read into a PC at a digitization rate of 4 kHz using Clampex 8 (Axon Instruments/Molecular Devices Corp, Union City, CA, USA). Large spikes (peak amplitude >15 or 20 pA) were used for PSF analysis, as these events are more likely to arise from release sites that are close to the recording electrode (Haller *et al.* 1998). This reduces the variability in PSF measurements. PSF lifetime was measured from onset to end point, as defined by the criteria of Chow & von Rüden (1995).

A previous study from this laboratory described a type of stand-alone foot with a mean amplitude of ~0.4 pA, which is much smaller than that of PSF (~2 pA) (Wang *et al.* 2003*a*). In the present study we focused attention on a different type of stand-alone foot with an amplitude close to that of PSF. Methods of analysis were developed here to distinguish these events from those full-fusion spikes that are distorted by diffusion (Haller *et al.* 1998). The durations of putative kiss-and-run events were analysed as follows. Once an event was identified, typically with peak amplitude >2 pA, the onset was taken as the time at which the current rose to 1 × RMS (root mean square) noise (~0.25 pA at 1 kHz) above the baseline current. This onset was identical to that used for PSF, as mentioned above. The end of a putative kiss-and-run event was taken as the time when the signal passed below the average amplitude of the points between the two preliminary time boundaries defined by the halfway points between baseline and peak. This duration is referred to as $t_1$ and is illustrated in traces in Fig. 3*C*. As an alternative measure of duration, we took the same starting point but used the time that the current returned to within 1 × RMS noise of the baseline current. This duration is referred to as $t_2$ and is also illustrated in traces in Fig. 3*C*. The ratio of these two times provided an index of event shape that was used to evaluate the rectangularity of putative kiss-and-run events.

The peak amplitude of an event was determined as the highest current value, and is an appropriate measure of amplitude for full-fusion spikes. However, this measurement is not appropriate for rectangular kiss-and-run events. For these events the mean amplitude is a better measure, and it was calculated using the area, determined by integrating from the start to the end points, and dividing by duration ($t_1$). In order to exclude the previously studied small-amplitude stand-alone-feet (Wang *et al.* 2003*a*), we used a cutoff of 2 pA for the peak amplitude (a 2 pA peak corresponds to a mean amplitude of 0.7 pA, which nicely separates the small stand-alone-feet (mean ~0.4 pA), from a new class of kiss-and-run events described here with mean amplitude of ~1.5 pA).

### Statistical analysis

The mean lifetime ($\tau$) of a PSF is computed as the arithmetic mean ($\overline{t}$) minus the cutoff time ($t_c$); $\tau = \overline{t} - t_c$, where $t_c$ is the limit below which events cannot be reliably detected, and $\overline{t}$ is computed for all events longer than

$t_c$. (This result is exact for an exponential distribution (Colquhoun & Sigworth, 1995)). Individual PSF lifetime measurements were multiples of the digitization interval of 0.25 ms, and we judged 1.0 ms as the shortest lifetime that could be reliably detected and accurately measured. This defined $t_c$ as the midpoint between 0.75 and 1.0, giving $t_c = 0.875$. Mean lifetimes estimated from single exponential fits to the cumulative distribution (Wang *et al.* 2001) by $\chi^2$ minimization (using Origin 5.0) differed by $<0.1$ ms from $\tau = \bar{t} - t_c$. The error estimate for $\tau$ was taken as the standard error of the arithmetic mean of the lifetimes, which equals the error in $\tau$ for a single exponential distribution determined by likelihood maximization (Colquhoun & Sigworth, 1995).

The spike amplitude shows a strong dependence on cells and/or recordings. For this reason we computed mean spike amplitude in two stages. First, the means were computed separately for each cell. Then these means were averaged to give what will be referred to as a double-mean, and the number of cells (rather than total number of events) was used to calculate the standard error (Colliver *et al.* 2000). Because event frequency and ratios of frequencies also vary between cells/recordings, these quantities were determined for individual cells and then averaged to produce a cell-mean. The Kruskal–Wallis non-parametric test and analysis-of-variance (GraghPad Instat version 3) indicated that there was no statistically significant dependence of PSF lifetime on cells/recordings, so that PSF lifetimes from many cells can be pooled for analysis as described above. Differences between means of different groups were evaluated for statistical significance with the Mann–Whitney test for two groups and the Kruskal–Wallis test for more than two groups.

## Results

### $Ca^{2+}$ dependence of release kinetics

Direct $Ca^{2+}$ application to permeabilized PC12 cells elicited vesicular release, which registered as spikes in amperometry traces (Fig. 1*A*). As in intact cells, spikes recorded in permeabilized cells are generally accompanied by PSF (Fig. 1*B*), and the lifetimes of these fusion pore events follow an exponential distribution (Fig. 1*C*). A single exponential provided a good fit for all concentrations of $Ca^{2+}$ tested, indicating that permeabilization leaves fusion pore dynamics qualitatively similar. The similarity becomes quantitative if we assume that depolarization of intact cells raises intracellular $[Ca^{2+}]$ to 1–2 $\mu$M (Wang *et al.* 2001, 2003*a*). The mean PSF lifetime decreased with increasing $[Ca^{2+}]$, indicating that $Ca^{2+}$ influences the stability of open fusion pores (Fig. 1*D*). Thus, $Ca^{2+}$ interacts with the fusion apparatus during the actual exocytosis of vesicles. This action is probably mediated by Syt, which has been shown to influence fusion pore stability (Wang *et al.* 2001).

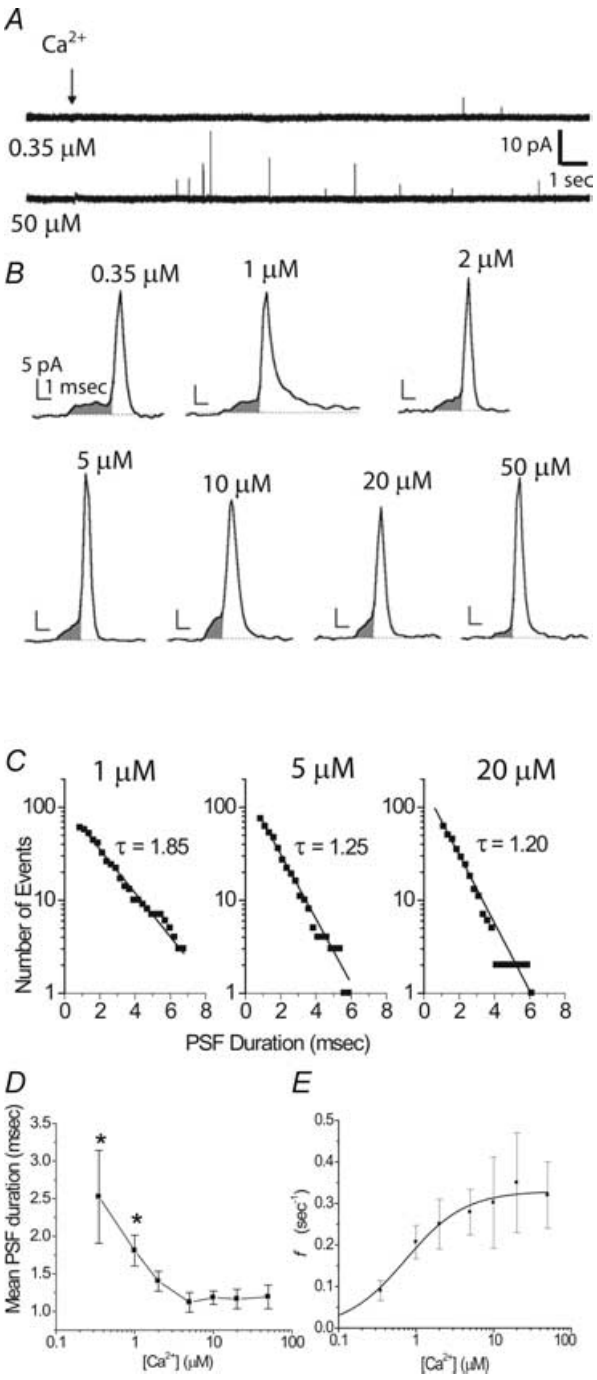


**Figure 1. $Ca^{2+}$-triggered amperometric spikes from permeabilized PC12 cells**
*A*, the indicated concentrations of $Ca^{2+}$ were applied at the arrow, triggering release from permeabilized cells transfected with Syt I cDNA. *B*, expanded traces show PSF as shaded regions. *C*, PSF lifetime distributions for the indicated $[Ca^{2+}]$ (60–152 PSF events, 17–31 cells and 6–7 transfections for each $[Ca^{2+}]$). *D*, mean PSF duration ($\tau$) is plotted *versus* $[Ca^{2+}]$. * indicates $P < 0.05$ for comparison against pooled data from $[Ca^{2+}] \geq 5$ $\mu$M. *E*, frequency of spikes (peak >3.5 pA; see Fig. 3*D* and Methods) is plotted *versus* $[Ca^{2+}]$. A fit to the Hill equation gave $V_{max} = 0.33 \pm 0.02$ s$^{-1}$, $EC_{50} = 0.74 \pm 0.13$ $\mu$M, $n_H$(Hill coefficient) $= 1.13 \pm 0.25$ ($\chi^2 = 0.00038$).

According to a minimal model for the kinetics of fusion pores, closed pores assemble and open. Open fusion pores can then either close or dilate (Wang *et al.* 2001).

$$\xrightarrow{k_a} C \underset{k_c}{\overset{k_o}{\rightleftharpoons}} O \xrightarrow{k_d} D$$

*C*, *O*, and *D* represent closed, open, and dilating fusion pores, respectively. $k_a$ represents the rate constant for fusion pore assembly, $k_o$ is the rate of opening, $k_c$ is the rate of closing, and $k_d$ is the rate of entering a dilating state. The mean PSF lifetime depends only on the closing and dilating rate constants:

$$\tau = \frac{1}{k_c + k_d} \quad (1)$$

Thus, the $[Ca^{2+}]$ dependence of $\tau$ shown in Fig. 1*D* indicates that the sum of $k_c$ and $k_d$ increases as $[Ca^{2+}]$ increases. This suggests that $Ca^{2+}$ binding accelerates at least one of these fundamental rate processes.

An indication that $k_d$ rather than $k_c$ expresses the $[Ca^{2+}]$ dependence of $\tau$ is provided by an analysis of spike frequency. We previously reported that increasing $[Ca^{2+}]$ increased the spike frequency in permeabilized cells (Wang *et al.* 2003*a*). In this earlier study we plotted all events with a peak amplitude >2 pA. Due to new results to be presented later in this article, we now know that using this cutoff results in the inclusion of kiss-and-run events arising from the same fusion pore that produces PSF. To avoid including these events, we plotted the frequency of events with peak amplitudes >3.5 pA (Fig. 1*E*). This allows us to focus on spikes that follow pore dilation, the frequency of which can be written as

$$f = \frac{f_o k_d}{k_c + k_d} \quad (2)$$

where $f_o$ is the frequency of fusion pore openings within a region of the cell that is close enough to the electrode for detection.

Eqns (1) and (2) allow us to interpret the $[Ca^{2+}]$ dependence of $\tau$ (Fig. 1*D*) and $f$ (Fig. 1*E*) in terms of the basic rate constants that appear in our kinetic scheme for the fusion pore. It is notable that an increase in $k_d$ with $[Ca^{2+}]$ is consistent with both the observed decrease in $\tau$ (eqn (1)) and the increase in $f$ (eqn (2)). By contrast, if $k_c$ varies with $[Ca^{2+}]$ then the two measured quantities $f$ and $\tau$ would show a positive correlation. Since the increase in $f$ is accompanied by a decrease in $\tau$, it is easier to account for the changes in both of these quantities with changes in $k_d$. The inverse correlation between $\tau$ and $f$ is illustrated in the Supplemental material, along with a more detailed kinetic analysis. The $[Ca^{2+}]$ dependence of these rate constants will be assessed more directly below (Fig. 6*A*). It is significant that changes solely in $k_c$ or $f_o$ are inconsistent with the observation of both the decrease in $\tau$ and the increase in $f$ with $[Ca^{2+}]$.

### Effects of mutations on release kinetics

In a complementary approach to the analysis of the $Ca^{2+}$ dependence of fusion pore kinetics, we studied mutants of Syt I, in which $Ca^{2+}$ binding to the C2A or C2B domains was impaired. cDNA encoding the Syt I mutants D230S and D363N were transfected into PC12 cells to study the effects of $Ca^{2+}$ ligand replacements on exocytosis. D230S is a $Ca^{2+}$-binding site mutation in the C2A domain (designated C2A*) and D363N is a $Ca^{2+}$-binding site mutation in the C2B domain (designated C2B*). Each mutated residue forms the first ligand of the third loop of the $Ca^{2+}$-binding pocket of its C2 domain (Ubach *et al.* 1998). Recombinant protein that includes the entire cytoplasmic region and both of the C2 domains was tested for binding to liposomes containing phosphatidyl serine (PS) and phosphatidyl inositol biphosphate ($PIP_2$), as well as for binding to heterodimeric complexes of the t-SNAREs, SNAP-25 and syntaxin (Supplemental material). Both C2A* and C2B* cytoplasmic domains showed greatly reduced binding to PS-containing liposomes and t-SNARE heterodimer, but only C2B* showed reduced binding to $PIP_2$-containing liposomes.

Amperometry recording revealed single-vesicle release events in intact PC12 cells transfected with cDNA encoding wild-type Syt I as well as cDNA encoding C2A* and C2B* (Fig. 2*A*). Both mutants reduced exocytosis compared to that seen in cells transfected with wild-type Syt I cDNA. Wild-type Syt I left the frequency of spikes identical to that seen in control cells (Wang *et al.* 2001). Transfection with cDNA encoding C2B* reduced the frequency of release events by 5.9-fold compared to a 2.6-fold reduction seen with C2A* (Fig. 2*B* and *C*). This difference might be related to a greater dependence of $PIP_2$ binding (Bai *et al.* 2004*a*) and Syt I oligomerization (Wu *et al.* 2003) on the C2B domain.

C2A* had no effect on the mean PSF lifetime (Fig. 2*D*). The value of $\tau = 1.62 \pm 0.26$ ms ($n = 35$) was indistinguishable from the value of $1.60 \pm 0.10$ ms ($n = 201$) for wild-type Syt I (this value includes data obtained in parallel with the mutants studied here as well as control data from earlier studies (Wang *et al.* 2001)). Other mutations that produce a modest reduction in the $Ca^{2+}$-binding functions of the C2A domain also have no effect on the mean PSF lifetime (Sorensen *et al.* 2003; Wang *et al.* 2003*b*). By contrast, the C2B* mutant reduced $\tau$ to $0.70 \pm 0.29$ ms ($n = 23$; $P = 0.02$; Fig. 2*D*) compared with the values of 1.60 and 1.62 ms for wild-type Syt I and C2A*, respectively.

C2A* had no effect on the mean peak amplitude of single-vesicle release events, but C2B* reduced the mean peak amplitude by more than half (Fig. 2*E*). The area of single-vesicle release events showed a similar reduction ($P < 0.001$ compared to Syt I, data not shown). The conventional interpretation of such a reduction is that the

content of a vesicle is reduced. However, it is difficult to see how a mutation in Syt I would alter the content of a vesicle. In the following section we will explore the more plausible interpretation that this reduction arises from a greater frequency of kiss-and-run events, in which fusion pores open to produce a current amplitude similar to that of PSF, but then close without dilating.

### Kiss-and-run with a C2B mutation

Amperometry recordings from PC12 cells transfected with *C2B** cDNA revealed a large number of small events with approximately rectangular shapes (Fig. 3*Aa*). These events were similar in amplitude to PSF (Fig. 3*Ab*), and were ∼4× larger than the 0.4 pA rectangular events (Fig. 3*Ac*) that reflect a distinct, exclusively kiss-and-run exocytotic pathway that becomes more prevalent in cells with elevated levels of Syt IV (Wang *et al.* 2003*a*). Since a rectangular shape is an important hallmark of kiss-and-run exocytosis (Álvarez de Toledo *et al.* 1993; Albillos *et al.* 1997; Ales *et al.* 1999; Wang *et al.* 2003*a*), the events displayed in Fig. 3*Aa* suggest that the ∼2 pA fusion pores that give rise to PSF are able to close without dilating. We therefore analysed these events further in order to determine whether they constitute a distinct population with the properties expected for kiss-and-run release through the fusion pore of the PSF. In data from the *C2B** mutation, the higher proportion of rectangular events was very helpful in developing approaches to data analysis that could then be applied to data from wild-type Syt I, where the lower incidence of rectangular events made classification based on direct visual examination of amperometry records more difficult (Wang *et al.* 2001, 2003*a*).

Since a higher proportion of these rectangular events could account for the reduced mean spike amplitude with C2B* just mentioned (Fig. 2*E*), we examined distributions of peak event amplitude. In cells transfected with wild-type Syt I cDNA (Fig. 3*Ba*) the amplitudes were spread out broadly above ∼4 pA, but there was a narrow cluster of events with a peak at ∼2.4 pA. There was also a small peak at ∼1 pA, and these smaller events resulted from a different form of kiss-and-run previously described (Wang *et al.* 2003*a*). These events are actually much smaller in amplitude than the ∼1 pA peak indicated in Fig. 3*Ba*. In our previous study it was necessary to filter records at 100 Hz to reduce the RMS noise to ∼0.1 pA and reveal these events clearly, but with the present bandwidth of 1 kHz the RMS noise was ∼0.25 pA. With many of these events thus hidden, we saw only the edge of the population for which the mean amplitude is ∼0.4 pA.

The distribution for the *C2B** mutation (Fig. 3*Bb*) had the same basic feature of three groupings seen with wild-type Syt I, but with a smaller contribution from the broadly distributed population above 4 pA. The comparison of these two plots indicates that the *C2B** mutation alters the distribution of amplitudes by increasing the proportion of small events centred at 2.4 pA. This difference is especially clear when the two cumulative distributions are normalized to total number of events and plotted together (Fig. 3*Bc*).

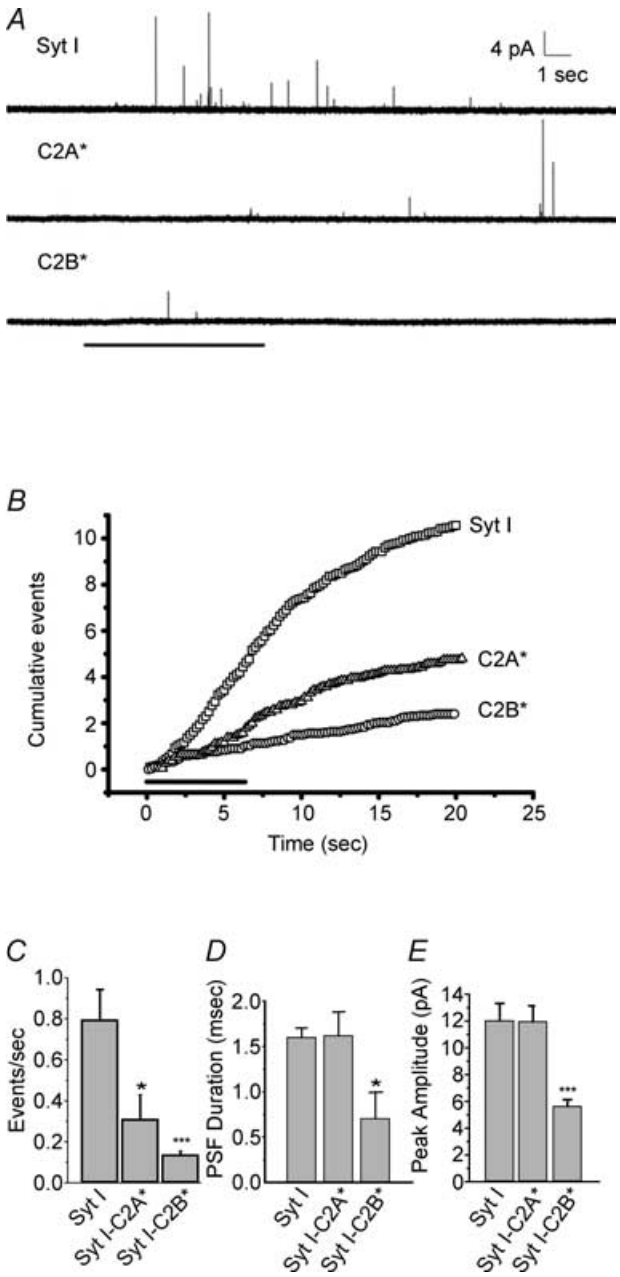


**Figure 2. Amperometry recordings from intact transfected cells**
*A*, amperometry recordings from intact cells transfected with Syt I cDNA, and Syt I cDNA harbouring mutations in the $Ca^{2+}$-binding sites of the C2A and C2B domains (D230S = C2A* and D363N = C2B*). Secretion was triggered with a high-KCl solution (see Methods) applied as indicated by the bar. *B*, cumulative event count (events >2 pA peak) per cell is plotted *versus* time, in cells transfected with cDNA encoding Syt I (□), C2A* (△), and C2B* (○). *C*, frequencies of events with peaks >2 pA for the indicated form of Syt I were determined for each cell and averaged. *D*, mean PSF durations for the indicated proteins. *$P < 0.05$; *** $P < 0.001$. Data from 37 to 38 cells and 5–8 transfections for each protein. *E*, mean peak amplitudes for the indicated protein (double-means, see Methods).

If the peaks near 2.4 pA in the distributions in Figs 3*Ba* and 3*Bb* reflect predominantly vesicles undergoing kiss-and-run rather than full-fusion, then these events should have a more rectangular shape compared with the spike-like full-fusion events. To evaluate event shape we compared two different measures of event duration, indicated as $t_1$ and $t_2$ in Fig. 3*C*. $t_1$ is defined as the duration from the onset until the time at which the amplitude falls below the mean amplitude of the points falling within the half-width of the event (see Methods).

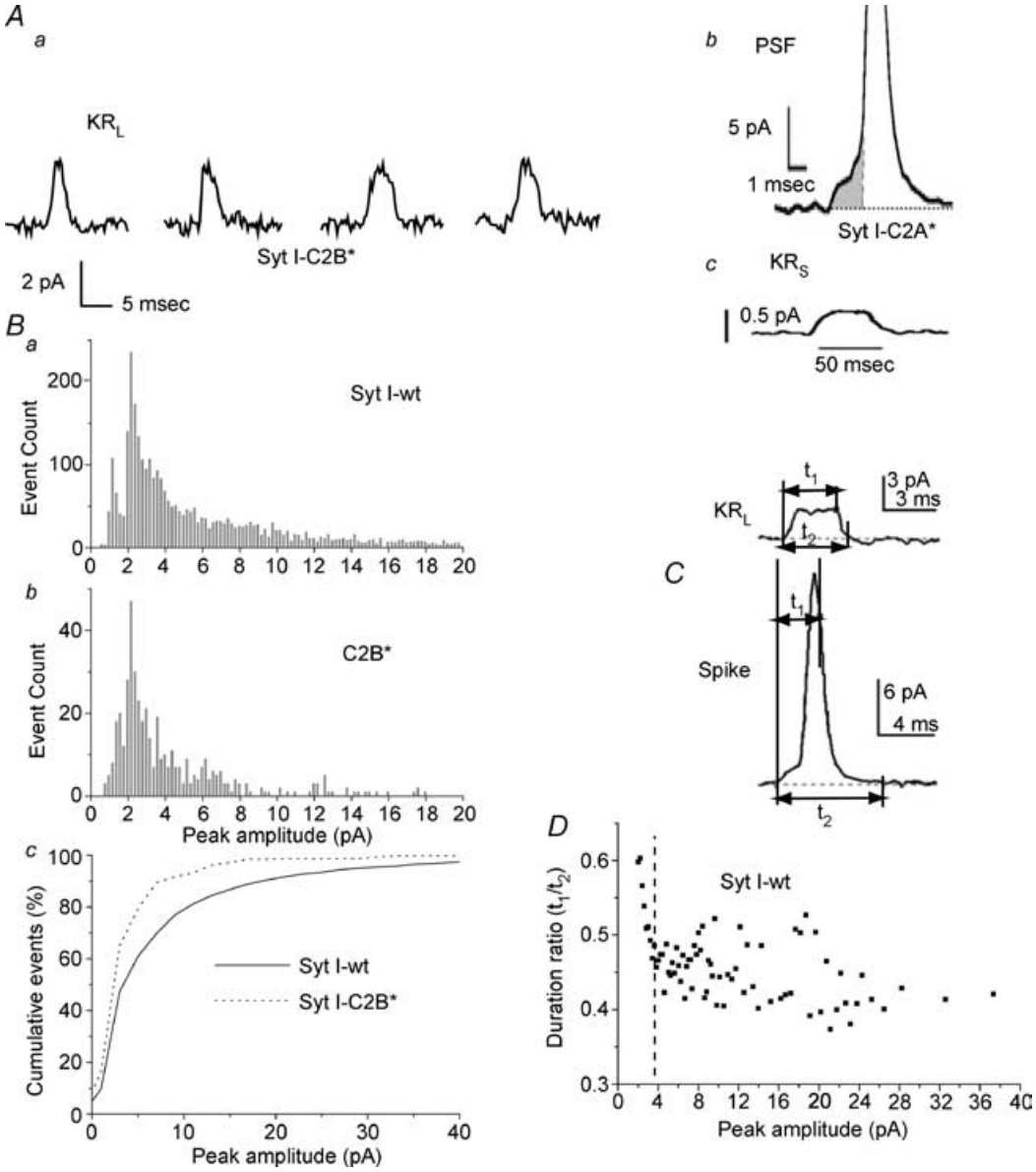


**Figure 3. Kiss-and-run events**
*Aa*, large kiss-and-run events ($KR_L$) recorded from PC12 cells transfected with Syt I C2B* cDNA. *Ab*, a spike with a prespike foot (PSF). *Ac*,. a small kiss-and-run event ($KR_S$) (Wang *et al.* 2003*a*); this recording was made with a 100 Hz low-pass filter. *Ab* and *Ac* are from PC12 cells transfected with Syt I C2A* cDNA. *Ba*, peak amplitude distributions were plotted for wild-type Syt I (Syt I-wt) and *Bb*, the C2B* mutation (Syt I–C2B*). There were 1985 total events from 74 cells for wild-type Syt I and 313 total events from 38 cells for C2B*. *Bc*, the two distributions from *Ba* and *Bb* are plotted in a cumulative form and normalized to the total number of events. *C*, two different measures of duration, $t_1$ and $t_2$, are shown for a $KR_L$ event and a spike. The onset in both cases is the point where the signal departs from baseline. For $t_1$ the end point is where the signal falls below the mean amplitude of the event (see Methods). For $t_2$ the end point is where the signal returns to baseline. The ratio $t_1/t_2$ is smaller for spike-shaped events than for rectangular events. *D*, the ratio $t_1/t_2$ was averaged for events with peak amplitudes in the same bin and plotted *versus* peak amplitude. The vertical line at 3.5 pA marks the cutoff employed for classifying events as either spikes (peak > 3.5 pA) or $KR_L$ (peak < 3.5 pA).

$t_2$ is defined as the duration starting at the same onset, but ending at the time the current returns to baseline. For a spike-like event, the second termination point is much later than the first, so $t_2$ will be much longer than $t_1$. For a rectangular event, the difference between the two end points reflects the duration of the steep final fall-off, so the difference between $t_2$ and $t_1$ will be less than for a spike. $t_2$ is ~25% larger than $t_1$ for the rectangular event of ~2.5 pA shown as the upper trace in Fig. 3*C*, and more than twice as large for the ~20 pA spike shown in the trace below. Calculating the ratio of $t_1/t_2$, and averaging for different peak amplitude bins shows that this ratio has a low value for peak amplitudes >3.5 pA, but rises sharply below 3.5 pA (Fig. 3*D*). This plot thus demonstrates a difference in shape between the large and small events, with a transition just below 3.5 pA. This result supports the hypothesis that the small-amplitude events associated with the peak at 2.4 pA in the distributions (Figs 3*Ba* and 3*Bb*) are more rectangular in shape compared with spikes.

As an additional test of the rectangular shape for small-amplitude events, we determined the duration, $t_1$, of events in the 2–3.5 pA peak amplitude range, and estimated mean amplitude as event area divided by duration. (It is important to reiterate the difference between *mean* amplitude and *peak* amplitude. Peak amplitude is an appropriate measure for spikes because they have a sharp apex. By contrast, the peak value has little meaning for flat rectangular events where the mean amplitude provides a better estimate. When classifying events by amplitude, we found it more convenient to use the peak. When amplitudes were compared to those of PSF, we used the mean amplitude and indicated that it corresponds to a given peak value.) A plot of the mean amplitude of each event *versus* its duration for 189 events from cells expressing C2B* was flat with no significant correlation (Fig. 4*A*, $P = 0.62$), as expected for rectangular events of uniform amplitude and variable lifetime. This behaviour is limited to small events. A plot for events >3.5 pA showed a strong inverse correlation ($P < 0.0001$, data not shown). The plot of PSF amplitude *versus* duration in cells transfected with wild-type Syt I cDNA was also flat with a slightly higher mean (Fig. 4*B*), and the plot of mean amplitude *versus* duration for all events in this range recorded from permeabilized cells transfected with wild-type Syt I cDNA (Fig. 4*C*) looked very much like the plot for C2B* (Fig. 4*A*). The somewhat larger mean amplitude of PSF reflects three sources of bias: (1) spikes were selected with peak amplitudes >20 pA; (2) the different shapes of PSF and putative kiss-and-run events had a small effect on their measured amplitudes; and (3) putative kiss-and-run events with peaks >3.5 pA were excluded.

Variations in the shape of single-vesicle fusion events partly reflect diffusion, as release from more distant sites gives rise to spikes that are broader and smaller. This effect produces a pronounced inverse correlation between amplitude and duration (Haller *et al.* 1998). As noted, this inverse correlation was highly significant for plots of events >3.5 pA, but the absence of a correlation in the plots shown in Fig. 4*A* and *C* indicates that these events are not full fusion spikes distorted by diffusion. The lack of dependence of mean amplitude on duration is

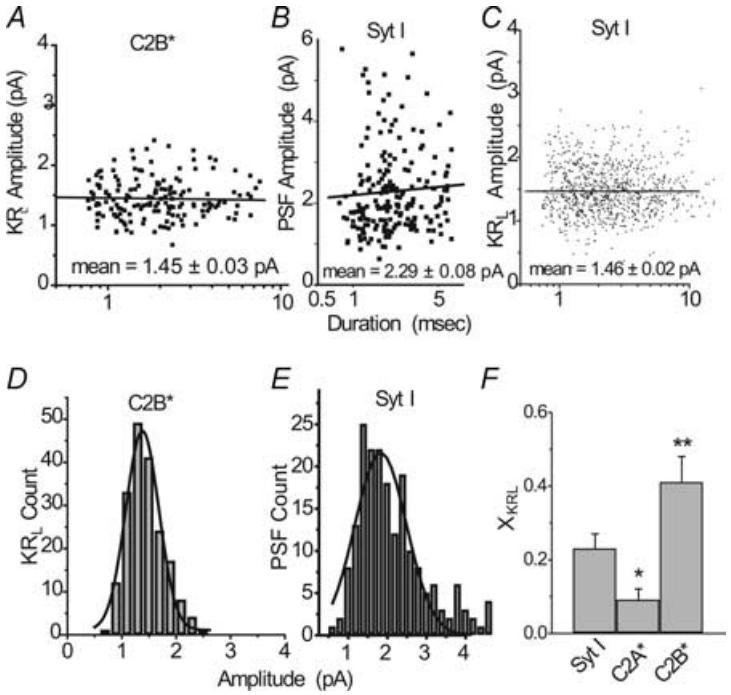


**Figure 4. Comparison of event amplitiudes for PSF and kiss-and-run events**
*A*, plot of amplitude *versus* duration for events in the 2–3.5 pA peak amplitude range ($KR_L$) for recordings from cells transfected with *C2B** cDNA (198 events). *B*, plot of amplitude *versus* duration for PSF recorded from cells transfected with Syt I cDNA (201 events). *C*, plot of amplitude *versus* duration for events in the 2–3.5 pA peak amplitude range ($KR_L$) for recordings of $Ca^{2+}$-evoked release from permeabilized cells transfected with wild-type Syt I cDNA (936 events). The best-fitting lines are shown with slopes determined from the fits. Linear regression gave $P = 0.62$, 0.42, and 0.97 for *A*, *B* and *C*, respectively. Distribution of amplitudes for Syt I–C2B* events (*D*) and Syt I PSF (*E*), with best-fitting Gaussians drawn as continuous curves. *F*, fraction of events ($X_{KR}$) with peak amplitudes in the range 2–3.5 pA relative to total >2 pA, for the indicated proteins (double-means, see Methods). $^*P < 0.05$; $^{**}P < 0.01$ in the comparison with wild type. Data were from 37 to 38 cells and 5–8 transfections for intact cells transfected with wild-type or mutant Syt I cDNA and 164 cells and >50 transfections for permeabilized cells transfected with wild-type Syt I cDNA.

indicative of a rectangular shape, and therefore supports the identification of these events as kiss-and-run.

The distribution of mean amplitudes within the 2–3.5 pA peak amplitude range for C2B* was well fitted by a Gaussian function centred at $1.38 \pm 0.02$ pA (Fig. 4*D*), further indicating that these events are a distinct population rather than the tail of the distribution of larger full-fusion spikes. This distribution resembles that of PSF amplitudes in Syt I-transfected cells, although for reasons already mentioned, the mean amplitude from a Gaussian fit was significantly higher ($1.80 \pm 0.05$ pA for Fig. 4*E*; $P < 0.001$). The durations of the putative kiss-and-run events were $\tau = 2.39 \pm 0.07$ ms ($n = 813$) and $1.30 \pm 0.13$ ms ($n = 189$) in intact cells transfected with Syt I and *C2B** cDNA. These values are somewhat larger that the values of the corresponding PSF mean durations, and we are unable to say whether this is a real difference or a reflection of the greater difficulty of detecting brief kiss-and-run events.

These comparisons indicate that events with peak amplitudes in the range 2–3.5 pA (mean 0.7–2.5 pA) in cells transfected with cDNA encoding the C2B* mutations are fusion pore openings that close without resolving to spikes. We therefore designated them as large kiss-and-run events ($KR_L$). These $KR_L$ are distinct from the small 0.4 pA (mean amplitude) kiss-and-run events reported previously (Wang *et al.* 2003*a*), which we now call $KR_S$. With reference to the minimal kinetic scheme of Wang *et al.* (2001) employed above to interpret the $Ca^{2+}$ dependence of PSF lifetime and spike frequency, these $KR_L$ events reflect fusion pores that go through a $C \rightarrow O \rightarrow C$ sequence, rather than the than the $C \rightarrow O \rightarrow D$ spike sequence.

To quantify the fraction of $KR_L$ *versus* full-fusion spikes, we selected a peak current amplitude as a boundary, and classified smaller events as $KR_L$ and larger events as spikes. All events <2 pA (mean 0.7 pA) were omitted in order to exclude $KR_S$ events (Wang *et al.* 2003*a*). Based on the extent of the $KR_L$ peak in the amplitude distributions (Fig. 3*Ba* and *b*) and on the transition in the plot of a rectangular shape index ($t_1/t_2$ in Fig. 3*D*), we considered that a peak amplitude in the range of 3.5–4 pA would effectively separate spikes from $KR_L$. We tested both 3.5 and 4 pA, and found that the results of the analysis were not sensitive to this choice because the actual number of events in this range is <10% of the total. We decided to use 3.5 pA in order to be more conservative about classifying $KR_L$, using the range 2–3.5 pA (0.7–2.5 pA mean) for $KR_L$ and >3.5 pA for spikes. The fraction of $KR_L$ events ($X_{KR} = KR_L/(KR_L + \text{spikes})$) is indicated in Fig. 4*F*. Cells transfected with cDNA encoding the C2B* mutation had twice as large a fraction of $KR_L$ compared to wild-type Syt I. In cells transfected with DNA encoding the C2A* mutation, this fraction was reduced by a factor of more than two. Taking into account this higher proportion of $KR_L$ relative to spikes indicates that the 5.9-fold reduction in total event frequency for C2B* relative to wild-type Syt I (Fig. 2*C*) converts to a larger, 7.7-fold reduction in the frequency of full-fusion spikes. The same correction for C2A* changes the factor by which spike frequency is reduced from 2.6 to 2.2.

The high proportion of $KR_L$ seen with C2B* indicates that this mutation arrests fusion at the open fusion pore. This suggests that $Ca^{2+}$ binding to the C2B domain drives fusion pore dilation. In terms of the kinetic model used above to analyse the $Ca^{2+}$ dependence of fusion pore lifetime, the effect of the mutation could reflect either a decrease in the rate of fusion pore dilation, $k_d$, or an increase in the rate of fusion pore closure, $k_c$. An analysis presented below uses measurements of $\tau$ and the fraction of $KR_L$ to determine how each of these rate constants is altered.

### $Ca^{2+}$ dependence of $KR_L$ events

Although $KR_L$ events account for a smaller fraction of the total in cells transfected with wild-type Syt I cDNA than in cells transfected with *C2B** cDNA, they have the same fundamental properties. The mean amplitude of 1.46 pA (Fig. 4*C*) was similar to that of the $KR_L$ events seen with C2B* mutants (1.45 pA, Fig. 4*A*), and the mean amplitude was uncorrelated with duration (Fig. 4*A* and *C*). We therefore returned to the recordings from permeabilized cells transfected with Syt I cDNA. If raising $[Ca^{2+}]$ reduces the PSF duration because $Ca^{2+}$ triggers fusion pore dilation (Fig. 1*D*), we would expect $KR_L$ events to be more frequent at low $[Ca^{2+}]$. This was confirmed in two ways. First, a greater proportion of $KR_L$ events should reduce the mean event amplitude, and in fact it was significantly lower at low $[Ca^{2+}]$ (Fig. 5*A*). This result is reminiscent of the reduced mean amplitude of events recorded from cells expressing C2B* (Fig. 2*E*). This observation does not depend on the subdivision of events into spikes and $KR_L$, and is therefore a particularly strong demonstration of an effect of $Ca^{2+}$ on fusion pore kinetics.

In a second approach, we examined the $KR_L$ events more directly by subdividing all events into the same amplitude groups used in Fig. 4*F*, and calculated the proportion of events in the 2–3.5 pA range as the fraction of $KR_L$, $X_{KR}$. There was a clear decrease in this quantity as $[Ca^{2+}]$ was raised (Fig. 5*B*). These results indicate that the $KR_L$ events seen in permeabilized cells constitute a larger fraction of the observed events at low $[Ca^{2+}]$.

### Kinetic analysis of $[Ca^{2+}]$ dependence

The $[Ca^{2+}]$ dependence of PSF lifetime, $\tau$ (Fig. 1*D*), together with the fraction of kiss-and-run events, $X_{KR}$ (Fig. 5*B*), can be used to evaluate the rate constants, $k_d$ and $k_c$ in the kinetic scheme employed above. In our original

use of this model, the fusion pore-closing step with a rate constant of $k_c$ was included for completeness (Wang *et al.* 2001), but at that time we had no direct evidence for the occurrence of this transition. The $KR_L$ events revealed here demonstrate that these transitions do occur.

The kinetic scheme gives the fraction of $KR_L$ in terms of the rate constants as

$$X_{KR} = k_c/(k_d + k_c) \quad (3)$$

This relation together with eqn (1) makes it possible to solve for $k_d$ and $k_c$. The values are plotted in Fig. 6*A* and *B*. As anticipated from our analysis of $\tau$ and $f$ (Fig. 1*D* and *E* and supplemental material), $k_d$ increased with increasing $[Ca^{2+}]$ (Fig. 6*A*). By contrast, $k_c$ had no significant $[Ca^{2+}]$ dependence (Fig. 6*B*; $P = 0.10$ from linear regression). We also determined the total frequency of events >2 pA (Fig. 6*C*) from the data of Wang *et al.* (2003*a*), but here the frequency was computed as a double-mean (Colliver *et al.* 2000; Methods). The plot in Fig. 6*C* differs from the frequency of larger spikes plotted in Fig. 1*E* because it represents the sum of both full-fusion spikes and $KR_L$, and is thus the frequency of all fusion pore openings, including openings that either close or dilate. This total frequency of fusion pore openings was referred to above as $f_o$.

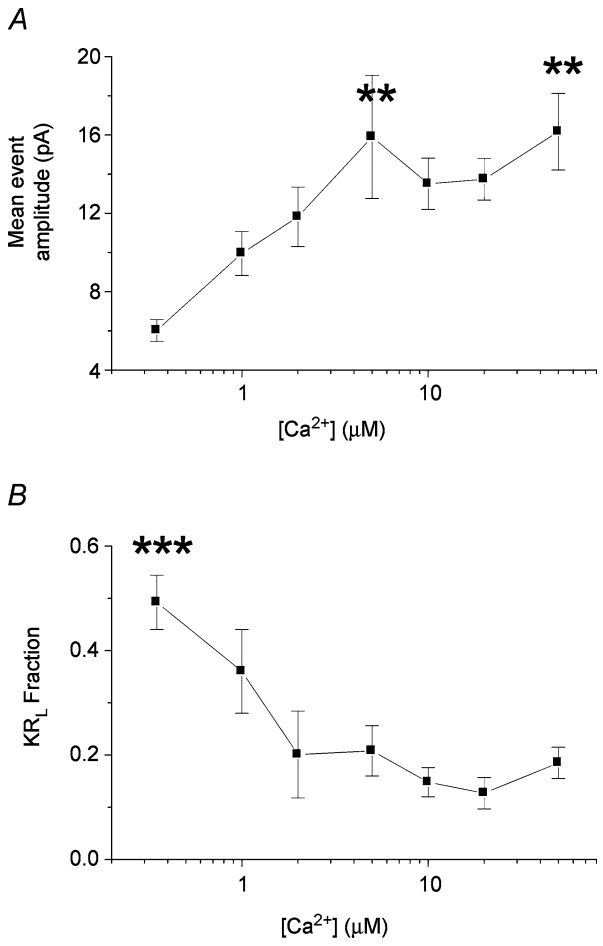


**Figure 5. $Ca^{2+}$ dependence of spike amplitude and fraction of kiss-and-run events**
*A*, $Ca^{2+}$ dependence of mean event amplitude (double-mean of events with peak amplitude >2 pA, see Methods). $^{**}P < 0.01$ for comparison with $[Ca^{2+}] = 0.35$ $\mu$M. *B*, the fraction of $KR_L$ events, $X_{KR}$, plotted *versus* $[Ca^{2+}]$. $X_{KR}$ was computed as the number of events in the 2–3.5 pA range, divided by all events >2 pA. Error bars are the standard error of the mean, where the fraction was computed for each cell and then averaged. $^{***}P < 0.001$ for comparison with $[Ca^{2+}] > 1$ $\mu$M. Data were from 17 to 31 permeabilized cells and 6–7 transfections.

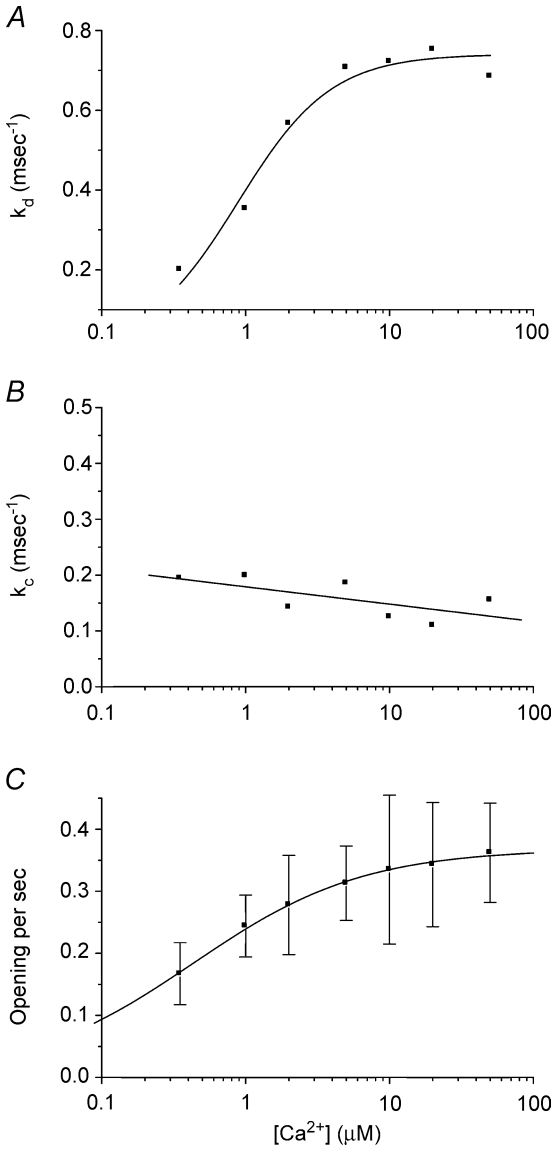


**Figure 6. $Ca^{2+}$ dependence of fusion pore kinetics in permeabilized Syt I-transfected cells**
*A*, the dilation rate, $k_d$, *B*, closing rate, $k_c$, and *C*, fusion pore-opening frequency, $f_o$ are plotted *versus* $[Ca^{2+}]$. The best-fitting Hill equations are drawn in *A* and *C*; the best-fitting line ($P = 0.10$ from linear regression) is drawn in *B*. For *A*, $k_{d\text{-max}} = 0.74 \pm 0.03$, $EC_{50} = 0.90 \pm 0.13$ $\mu$M, $n_H = 1.35 \pm 0.27$. For *C* $f_{o\text{-max}} = 0.37 \pm 0.01$ $s^{-1}$, $EC_{50} = 0.43 \pm 0.03$ $\mu$M, $n_H = 0.74 \pm 0.05$ ($\chi^2 = 0.00002$).

**Table 1. Rate constants for fusion pore closing ($k_c$) and dilation ($k_d$) calculated from measured values of fusion pore lifetime ($\tau$) and fraction of kiss-and-run events ($X_{KR}$), using eqns (1) and (3)**

| | Rate constants ($ms^{-1}$) | |
|---|---|---|
| | $k_c$ | $k_d$ |
| Syt I | 0.14 | 0.49 |
| C2A* | 0.056 | 0.56 |
| C2B* | 0.58 | 0.84 |

C2A* and C2B* denote the Syt I mutations of $Ca^{2+}$ ligands in the C2A domain and the C2B domain, respectively.

The plot of $k_d$ (Fig. 6*A*) was fitted to the Hill equation, yielding $k_{d\text{-}max} = 0.74 \pm 0.03\ ms^{-1}$, $EC_{50} = 0.90 \pm 0.13\ \mu M$, and $n_H$ (the Hill coefficient) $= 1.35 \pm 0.27$. For the plot of $f_o$ (Fig. 6*C*) a fit to the Hill equation yielded $f_{o\text{-}max} = 0.37 \pm 0.01\ s^{-1}$, $EC_{50} = 0.43 \pm 0.03\ \mu M$, and $n_H = 0.74 \pm 0.05$ (Wang *et al.* 2003*a*). These results thus resolve fusion pore opening and fusion pore dilation ($k_d$) as two distinct $Ca^{2+}$-dependent processes with the capability of making independent contributions to $Ca^{2+}$-triggered exocytosis. The $EC_{50}$ values and Hill coefficients for the $Ca^{2+}$ dependence of $k_d$ and $f_o$ are different. Thus, these two $Ca^{2+}$-triggered steps exhibit different $Ca^{2+}$-sensing properties. The higher $EC_{50}$ value for $k_d$ assures the occurrence of kiss-and-run events at low $[Ca^{2+}]$.

### Kinetic analysis of C2A and C2B mutants

We applied the same form of analysis to $\tau$ and $X_{KR}$ from cells in which release was triggered from intact cells by KCl depolarization. This analysis yielded values for $k_c$ and $k_d$ for wild-type Syt I and the two Syt I mutants (Table 1). The wild-type Syt I value for $k_c$ was close to the mean of the values plotted in Fig. 6*B*. The $k_d$ value is between the values of the points plotted at 1 and 2 $\mu M$ $[Ca^{2+}]$ (Fig. 6*A*), thus falling in the range for intracellular $[Ca^{2+}]$ estimated in intact PC12 cells depolarized with KCl (Wang *et al.* 2003*a*). The values in Table 1 indicate that the reduction in $X_{KR}$ for the $Ca^{2+}$ ligand mutation in the C2A domain (Fig. 4*F*) results primarily from a decrease in $k_c$. C2B* changed both of these rates. This mutation accelerated both of the open fusion pore exit rates, but $k_c$ showed the greatest change. $k_c$ appears to be especially sensitive to $Ca^{2+}$ ligand mutations in Syt I. Other mutations that selectively weaken Syt I binding to t-SNAREs reduced exocytosis in a manner consistent with an increase in $k_c$ (Bai *et al.* 2004*b*).

## Discussion

Our analysis of fusion pores resolves exocytosis into a sequence of distinct steps, two of which respond to increases in $[Ca^{2+}]$. Both $Ca^{2+}$ and $Ca^{2+}$-ligand mutations in Syt I alter the stability and dynamics of fusion pores, as well as the frequency of fusion pore opening. The results with varying $[Ca^{2+}]$ and with mutations in Syt I both identify multiple $Ca^{2+}$-regulated steps, and the convergence of these two independent experimental approaches strengthens the general conclusion of dual sites of $Ca^{2+}$ control in the triggering of exocytosis. These observations provide insight into the specific steps of vesicle fusion that are controlled by $Ca^{2+}$ and Syt I, and can thus aid in the development of a detailed mechanism for how $Ca^{2+}$ binding to Syt I triggers exocytosis.

According to the present findings, the first of the $Ca^{2+}$-dependent steps entails the opening of a fusion pore, and the second entails its dilation. Both of these rate processes increased with $[Ca^{2+}]$, but with differences in the quantitative nature of the $[Ca^{2+}]$ dependence. By contrast, the rate constant for fusion pore closure had no significant dependence on $[Ca^{2+}]$, suggesting that this is a first-order kinetic process of open fusion pores. Thus, the return of open fusion pores to the closed state represented by this $Ca^{2+}$-independent rate constant $k_c$ reflects transitions initiated by a $Ca^{2+}$–Syt I complex, and may involve the dissociation of $Ca^{2+}$. As discussed further below, $k_c$ is sensitive to mutations in the $Ca^{2+}$-binding sites, and these mutations could exert their effect on $k_c$ by accelerating $Ca^{2+}$ release from the C2A and C2B domains.

The $Ca^{2+}$ dependence of the rate of fusion pore dilation is consistent with results from mast cells where higher $[Ca^{2+}]$ shortened the latency between fusion and release (Fernandez-Chacon & Alvarez de Toledo, 1995). These results are also consistent with the protracted decay of quantal synaptic currents at the *Drosophila* larval neuromuscular junction (Pawlu *et al.* 2004). It is interesting that high intracellular $[Ca^{2+}]$ favours full fusion, considering that high extracellular $[Ca^{2+}]$ favours kiss-and-run in chromaffin cells (Ales *et al.* 1999). However, very high Syt I levels in transfected PC12 cells may also be a factor in this comparison with wild-type chromaffin cells. Fusion pore fluctuations have been reported to increase with higher intracellular $[Ca^{2+}]$ (Zhou *et al.* 1996), but this result is difficult to relate to the kinetics of fusion pore transitions examined here.

Experiments with Syt I mutants indicated that both C2 domains of Syt I function in the first of these steps. Furthermore, the C2B domain subsequently stabilizes the open fusion pore, allowing more time for the next step of dilation. By contrast, the C2A domain has the opposite action, closing the fusion pore to promote kiss-and-run. These competing effects on the fusion pore reveal the choice between kiss-and-run and full fusion as a balance between forces exerted by the two C2 domains of Syt. Thus, as seen for the choice between a small fusion pore pathway and a large fusion pore pathway (Wang *et al.* 2003*a*), the choice within the large fusion pore pathway studied here is subject to regulation by Syt I in a manner that could vary with different Syt isoforms.

At two distinct points in exocytosis, disruption of the C2B domain has a greater impact than disruption of the C2A domain. A substantial body of work supports the idea that C2B domain impairment is more disruptive to exocytosis (Koh & Bellen, 2003; Nishiki & Augustine, 2004). The $Ca^{2+}$ ligands of both the C2A (Stevens & Sullivan, 2003) and C2B (Mackler *et al.* 2002; Nishiki & Augustine, 2004) domains participate in $Ca^{2+}$-triggered secretion, and the present analysis helps delineate the precise contributions made by each of these parts of the protein.

For a mutation in the C2B domain, open fusion pores were half as likely to dilate (Fig. 4*F*). Mutations were overexpressed on a wild-type background, raising the possibility that the few dilating spikes seen with C2B* reflect the action of wild-type Syt I. However, because the C2B mutation shortened the PSF lifetime (Fig. 2*D*), the mutant protein would appear to be participating in fusion in some way, rather than merely blocking it. The changes in fusion pore exit rates resulting from Syt I mutations are difficult to relate to the changes induced by $Ca^{2+}$ binding. Because $Ca^{2+}$ increases $k_d$, we would expect $k_d$ to fall when $Ca^{2+}$ binding is impaired, but with C2A* there was almost no change in $k_d$, and with C2B* there was a change in the opposite direction. A resolution of these puzzling results will require further study.

It is surprising that whereas both C2 domains influence exit rates from the open fusion pore, only the C2B domain mutation alters the PSF lifetime. The reason for this is that $k_c$ is smaller than $k_d$, and since the C2A mutation reduces $k_c$, the mean lifetime, $1/(k_c + k_d)$, is hardly affected, even though $k_c$ is reduced nearly 3-fold. This can explain reports that other mutations that alter $Ca^{2+}$ binding to the C2A domain fail to alter the fusion pore lifetime (Sorensen *et al.* 2003; Wang *et al.* 2003*b*). Mutations in the C2B domain are more effective in altering $\tau$ because they increase $k_c$. It is likely that the effect of different Syt isoforms on fusion pore lifetime (Wang *et al.* 2001) at least partly reflects the action described here of the C2B domain. Given the dependence of $Ca^{2+}$-dependent $PIP_2$ binding (supplemental data and Bai *et al.* 2004*a*) and oligomerization (Wu *et al.* 2003) on the C2B domain, these effectors are strong candidates for the Syt-mediated alterations in fusion pore kinetics. The finding that two distinct steps in exocytosis are controlled by $Ca^{2+}$ is interesting in light of the multiplicity of Syt I-binding interactions. The question of how $Ca^{2+}$-stimulated effector interactions mediate exocytosis has become controversial, and the resolution of this issue may require a greater appreciation of how different effector interactions perform in different steps of exocytosis.

Both the $EC_{50s}$ and Hill coefficients for the two $Ca^{2+}$-dependent steps (Fig. 6*A* and *C*) differed by a factor of about two. The sigmoidal $Ca^{2+}$ dependence of $k_d$ indicated that this action on fusion pore dilation is cooperative, whereas the $Ca^{2+}$ dependence of fusion pore opening ($f_o$) is not. The Hill coefficient for the $Ca^{2+}$ dependence of release varies quite a bit for reports using different experimental systems. The present results provide a possible explanation for this discrepancy. Variations in the exocytotic apparatus that speed up the non-cooperative, early step will allow the later, cooperative step to become rate limiting. The Hill coefficient will then reflect this cooperative process. In PC12 cells, the $Ca^{2+}$ dependence of exocytosis has a Hill coefficient of one or less (Earles *et al.* 2001; Wang *et al.* 2003*a*), suggesting that in these cells the rate-limiting step is the non-cooperative process of pore opening. A manipulation that increases $f_o$ could thus alter the apparent cooperativity of release by allowing fusion pore dilation to become rate limiting. Manipulations that bring about such a change need not act directly on the $Ca^{2+}$-sensing mechanism, but rather could influence either of the two processes to change which rate is limiting.

The present study focused on exocytosis mediated by fusion pores for which the amperometric current is ~2 pA. Another exclusively kiss-and-run pathway employs fusion pores for which the amperometric current is only ~0.4 pA (Wang *et al.* 2003*a*). The two pathways were previously represented by the following model, which we modify here to incorporate the present results on the roles of the C2A and C2B domains.

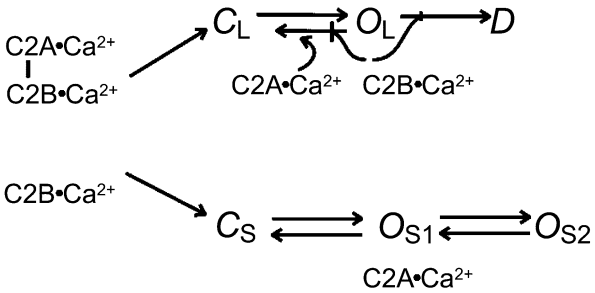


As in the designations of $KR_L$ and $KR_S$ above, the subscript L denotes large ~2 pA pores, and the subscript S denotes small ~0.4 pA pores. Note that the S pathway is exclusively kiss-and-run with no dilation step. We previously suggested that the C2B domain engages the S pathway and the C2A domain engages the L pathway, because manipulations that reduce $Ca^{2+}$ binding to the C2A domain divert traffic to the S pathway (Wang *et al.* 2003*a*). The present results show that mutating either the C2A or C2B domain reduces the frequency of L events, so we placed both domains at the entry to the L pathway. $Ca^{2+}$-triggered entry into the S pathway was cooperative and may require more than two $Ca^{2+}$ ions. The kinetic steps exiting $O_L$ also depend on the C2A and C2B domains, with the C2B domain slowing $k_c$ more than $k_d$, while the C2A domain accelerates $k_c$. The placement of the C2A domain in control of transitions between different pore states of the S pathway is based on alterations in

the multi-exponential fusion pore lifetime distribution following C2A manipulations (Wang *et al.* 2003*a*).

An interesting point that emerges from examining these two pathways together is that the order of engagement of the two C2 domains is partially reversed between the L pathway and the S pathway. Thus, when one of the C2 domains makes the initial step in generating a particular kind of fusion pore, the other C2 domain determines the next step. The two C2 domains may be flexible in terms of their effector interactions, with the ability to replace one another to produce different forms of exocytosis with different functional outcomes. This expands the capabilities of Syt, potentially endowing different isoforms with a repertoire of functions in the control of neurotransmitter release and synaptic transmission.

## References


Albillos A, Dernick G, Horstmann H, Almers W, Alvarez De Toledo G & Lindau M (1997). The exocytotic event in chromaffin cells revealed by patch amperometry. *Nature* **389**, 509–512.

Ales E, Tabares L, Poyato JM, Valero V, Lindau M & Alvarez De Toledo G (1999). High calcium concentrations shift the mode of exocytosis to the kiss-and-run mechanism. *Nature Cell Biol* **1**, 40–44.

Alvarez De Toledo G, Fernandez-Chacon R & Fernandez JM (1993). Release of secretory products during transient vesicle fusion. *Nature* **363**, 554–558.

Bai J, Tucker WC & Chapman ER (2004*a*). $PIP_2$ increases the speed of response of synaptotagmin and steers its membrane-penetration activity toward the plasma membrane. *Nature Struct Mol Biol* **11**, 36–44.

Bai J, Wang C-T, Richards DA, Jackson MB & Chapman ER (2004*b*). Fusion pore dynamics are regulated by synaptotagmin-t–SNARE interactions. *Neuron* **41**, 929–942.

Brose N, Petrenko AG, Südhof TC & Jahn R (1992). Synaptotagmin: a calcium sensor on the synaptic vesicle surface. *Science* **256**, 1021–1025.

Chapman ER (2002). Synaptotagmin: a $Ca^{2+}$ sensor that triggers exocytosis? *Nature Rev Mol Cell Biol* **3**, 498–508.

Chow RH & Von Rüden L (1995). Electrochemical detection of secretion from single cells. In *Single-Channel Recording*, ed. Sakmann B & Neher E, pp. 245–275. Plenum Press, New York.

Colliver TL, Hess EJ, Pothos EN, Sulzer D & Ewing AG (2000). Quantitative and statistical analysis of the shape of amperometric spikes recorded from two populations of cells. *J Neurochem* **74**, 1086–1097.

Colquhoun D & Sigworth F (1995). Fitting and statistical analysis of single channel records. In *Single-Channel Recording*, ed. Sakmann B & Neher E, pp. 483–587. Plenum Press, New York.

Earles CA, Bai J, Wang P & Chapman ER (2001). The tandem C2-domains of synaptotagmin contain redundant $Ca^{2+}$-binding sites that cooperate to engage t-SNAREs and trigger exocytosis. *J Cell Biol* **154**, 1117–1123.

Fernandez-Chacon R & Alvarez De Toledo G (1995). Cytosolic calcium facilitates release of secretory products after exocytotic vesicle fusion. *FEBS Lett* **363**, 221–225.

Fernandez-Chacon R, Königstorfer A, Gerber SH, Garcia J, Matos MF, Stevens CF, Brose N, Rizo J, Rosenmund C & Südhof TC (2001). Synaptotagmin I functions as a calcium regulator of release probability. *Nature* **410**, 41–49.

Fukuda M, Moreira JE, Lewis FM, Sugimori M, Niinobe M, Mikoshiba K & Llinas R (1995). Role of the C2B domain of synaptotagmin in vesicular release and recycling as determined by specific antibody injection into the squid giant synapse preterminal. *Proc Natl Acad Sci* **92**, 10708–10712.

Haller M, Heinemann C, Chow RH, Heidelberger R & Neher E (1998). Comparison of secretory responses as measured by membrane capacitance and by amperometry. *Biophys J* **74**, 2100–2113.

Hay J & Martin TFJ (1992). Resolution of regulated secretion into sequential MgATP-dependent and calcium-dependent stages mediated by distinct cytosolic proteins. *J Cell Biol* **119**, 139–151.

Jahn R & Südhof TC (1999). Membrane fusion and exocytosis. *Ann Rev Biochem* **68**, 863–911.

Klenchin VA, Kowalchyk JA & Martin TFJ (1998). Large dense-core vesicle exocytosis in PC12 cells. *Methods* **16**, 204–208.

Koh TW & Bellen HJ (2003). Synaptotagmin I, a $Ca^{2+}$ sensor for neurotransmitter release. *Trends Neurosci* **26**, 413–422.

Mackler JM, Drummond JA, Loewen CA, Robinson IM & Reist NE (2002). The C2B $Ca^{2+}$-binding motif of synaptotagmin is required for synaptic transmission in vivo. *Nature* **418**, 340–344.

Nishiki T-I & Augustine GJ (2004). Dual roles of the $C_2B$ domain of synaptotagmin in synchronizing $Ca^{2+}$-dependent neurotransmitter release. *J Neurosci* **24**, 8542–8550.

Pawlu C, DeAntonio A & Heckmann M (2004). Postfusional control of quantal current shape. *Neuron* **42**, 607–618.

Perin MS, Fried VA, Mignery GA, Jahn R & Südhof TC (1990). Phospholipid binding by a synaptic vesicle protein homologous to the regulatory region of protein kinase C. *Nature* **345**, 260–263.

Sorensen JB, Fernandez-Chacon R, Sudhof TC & Neher E (2003). Examining synaptotagmin 1 function in dense core vesicle exocytosis under direct control of $Ca^{2+}$. *J General Physiol* **122**, 265–276.

Stevens CF & Sullivan JM (2003). The synaptotagmin C2A domain is part of the calcium sensor controlling fast synaptic transmission. *Neuron* **39**, 299–308.

Tucker WC, Weber T & Chapman ER (2004). Reconstitution of $Ca^{2+}$-regulated membrane fusion by synaptotagmin and SNAREs. *Science* **304**, 435–438.

Ubach J, Zhang X, Shao X, Sudhof TC & Rizo J (1998). $Ca^{2+}$ binding to synaptotagmin: how many $Ca^{2+}$ ions bind to the tip of a C2-domain? *EMBO J* **17**, 3921–3930.

Wang C-T, Grishanin R, Earles CA, Chang P-Y, Martin TFJ, Chapman ER & Jackson MB (2001). Synaptotagmin modulation of fusion pore kinetics in regulated exocytosis of dense-core vesicles. *Science* **294**, 1111–1115.

Wang C-T, Lu J-C, Bai J, Chang P-Y, Martin TFJ, Chapman ER & Jackson MB (2003*a*). Different domains of synaptotagmin control the choice between kiss-and-run and full fusion. *Nature* **424**, 943–947.

Wang P, Wang C-T, Bai J, Jackson MB & Chapman ER (2003*b*). Mutations in the effector binding loops in the C2A and C2B domains of synaptotagmin I disrupt exocytosis in a nonadditive manner. *J Biol Chem* **278**, 47030–47037.

Wu Y, He Y, Bai J, Ji S, Tucker WC, Chapman ER & Sui S (2003). Visualization of synaptotagmin I oligomers assembled onto lipid monolayers. *Proc Natl Acad Sci* **100**, 2082–2087.

Zhou Z, Misler S & Chow RH (1996). Rapid fluctuations in transmitter release from single vesicles in bovine adrenal chromaffin cells. *Biophys J* **70**, 1543–1552.

## Acknowledgements

We thank Xue Han and David Richards for helpful discussions and comments. This work was supported by NIH grants NS30016 and NS44057 to MBJ and GM56827 and MH61876 to ERC. JB was supported by an AHA postdoctoral fellowship.

## Authors' present addresses

C.-T. Wang: Department of Biological Sciences, University of California, San Diego, CA, USA.
J. Bai: Department of Molecular Biology, Massachusetts General Hospital, Boston, MA, USA.

## Supplemental material

The online version of this paper can be accessed at:
DOI: 10.1113/jphysiol.2005.097378
http://jp.physoc.org/cgi/content/full/jphysiol.2005.097378/DC1
and contains supplemental material further kinetic analysis, and biochemical results for Syt-effector interactions.

This material can also be found as part of the full-text HTML version available from http://www.blackwell-synergy.com